

Self-masking in an Intact ERM-merlin Protein: An Active Role for the Central α -Helical Domain

Qianzhi Li¹, Mark R. Nance², Rima Kulikauskas³, Kevin Nyberg³
Richard Fehon³, P. Andrew Karplus⁴, Anthony Bretscher⁵
and John J. G. Tesmer^{2*}

¹Department of Chemistry
and Biochemistry, Institute for
Cellular and Molecular Biology
The University of Texas at
Austin 1 University Station
#A5300, Austin
TX 78712-0165, USA

²Life Sciences Institute
Department of Pharmacology
210 Washtenaw Ave.
University of Michigan
Ann Arbor, MI 48109, USA

³Department of Molecular
Genetics and Cell Biology
University of Chicago, Chicago
IL 60637, USA

⁴Department of Biochemistry
and Biophysics, Oregon State
University, Corvallis
OR 97331, USA

⁵Department of Molecular
Biology and Genetics, Cornell
University, Ithaca, NY 14853
USA

*Corresponding author

Ezrin/radixin/moesin (ERM) family members provide a regulated link between the cortical actin cytoskeleton and the plasma membrane to govern membrane structure and organization. Here, we report the crystal structure of intact insect moesin, revealing that its essential yet previously uncharacterized α -helical domain forms extensive interactions with conserved surfaces of the band four-point-one/ezrin/radixin/moesin (FERM) domain. These interdomain contacts provide a functional explanation for how PIP₂ binding and tyrosine phosphorylation of ezrin lead to activation, and provide an understanding of previously enigmatic loss-of-function missense mutations in the tumor suppressor merlin. Sequence conservation and biochemical results indicate that this structure represents a complete model for the closed state of all ERM-merlin proteins, wherein the central α -helical domain is an active participant in an extensive set of inhibitory interactions that can be unmasked, in a rheostat-like manner, by coincident regulatory factors that help determine cell polarity and membrane structure.

© 2006 Elsevier Ltd. All rights reserved.

Keywords: structure; actin; ERM; merlin; coiled-coil

Introduction

The plasma membrane is organized into functional regions, with the distinct apical and basolateral domains of polarized epithelial cells providing a well-studied example. To assemble, maintain and regulate the composition and structure of these domains, eukaryotes have evolved proteins that link the underlying cytoskeleton to specific membrane

proteins. Among the best understood class are the ezrin/radixin/moesin (ERM) family, which provide a conformationally regulated linkage from the cortical actin cytoskeleton to the plasma membrane, especially in structures like microvilli.^{1,2}

ERM proteins consist of three principal domains (Figure 1(a)). The best characterized of these are the band four-point-one/ezrin/radixin/moesin (FERM) domain³ and the C-terminal tail domain. The N-terminal ~300 residue FERM domain consists of three lobes, designated F1, F2 and F3, that are tightly associated in a cloverleaf-like structure.⁴ The FERM domain of ERM proteins binds directly to integral membrane proteins, such as CD43, CD44 and ICAM1-3, through their positively charged juxtamembrane regions,⁵⁻⁹ or indirectly through

Abbreviations used: ERM, ezrin/radixin/moesin; FERM, band four-point-one/ERM; Sfmoesin, moesin from *Spodoptera frugiperda*.

E-mail address of the corresponding author:
johntesmer@umich.edu

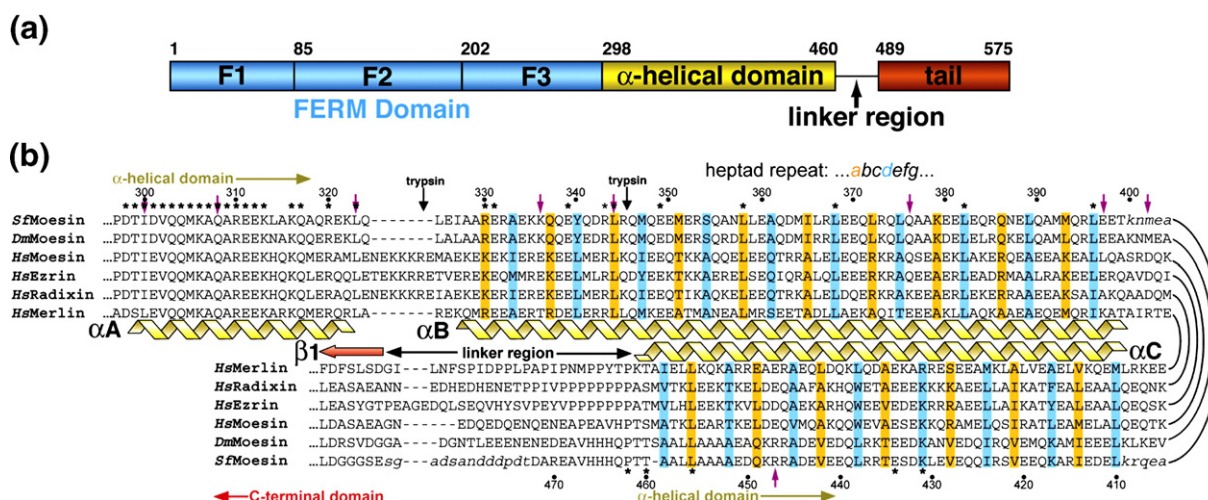


Figure 1. (a) Domain structure of Sfmoesin. Residue numbers at the domain boundaries are indicated. (b) Alignment of ERM-merlin α -helical domains. The sequence for α C is folded back (runs right to left) to indicate its register with the α B helix. Helical regions are indicated by a yellow coil, and the β 1 strand of the C-terminal tail by a red arrow. The *a* and *d* positions of the coiled-coil heptad repeat are shown with orange and cyan backgrounds, respectively.¹⁶ These positions interact with the other helix of the coil, as shown. Residues that are disordered in both Sfmoesin structures are shown with lower case italics. Sequence numbering corresponds to that of Sfmoesin, and the asterisks indicate invariant or highly conserved residues. Sites sensitive to trypsin digestion in the radixin α -helical domain (black arrows), and positions in human merlin associated with cancer (purple arrows) are indicated. Sequences used are as follows: human merlin (*HsMerlin*), SwissProt accession no. P35240; human radixin (*HsRadixin*), P35241; human ezrin (*HsEzrin*), P15311; human moesin (*HsMoesin*), P26038; and *D. melanogaster* moesin (*DmMoesin*), GenBank accession no. NP_996392.

the PDZ-containing scaffolding proteins EBP50/NHERF and E3KARP.^{10–12} The C-terminal tail domain (often referred to as the C-terminal tail or C-terminal ERM association domain or C-ERMAD) spans the last ~100 residues and contains an F-actin binding site in the last 30 residues.^{13–15} This domain interacts with the FERM domain as an extended, meandering polypeptide beginning with a β -strand associated with β 5 in F3 followed by four helices, the first two of which bind lobe F2 and second two of which bind lobe F3 (Figure 2(a)).⁴ The FERM-tail complex represents a dormant form of the protein in which membrane protein and active binding sites are masked.

Linking the FERM and C-terminal domains is an essential but structurally uncharacterized domain of ~190 residues, referred to as the α -helical domain, the most conserved feature of which being a heptad repeat characteristic of α -helical coiled-coils (Figure 1(b)).¹⁶ This region has been proposed to form an extended helical tether in activated ERM proteins linking the membrane-binding determinants of the FERM domain to the actin-binding determinant at the C-terminal tail.¹⁷ Although crystal structures have been reported for activated FERM domains as well as for the inactive FERM domain complexed with the C-terminal tail domain of human moesin, they have revealed at most only a small portion of the important and enigmatic α -helical domain.

Equally enigmatic is the neurofibromatosis 2 (NF2) tumor suppressor protein merlin, which is closely related to ERM proteins and shares all of the above features except for actin binding.^{18,19} Muta-

tions in merlin that lead to loss of tumor suppression are often disruptive, either truncating the protein or interfering with the proper fold of the protein. Some missense mutations of merlin associated with NF2 have been mapped to the interface of the FERM and C-terminal tail domain,⁴ suggesting that their association is critical for tumor suppressor activity. However, many more mutations remain unexplained, given the currently available models.

A particularly interesting aspect of ERM proteins is that they can exist in at least two conformational states,¹ an active open form with the FERM and C-terminal tail domain dissociated, and a dormant closed form similar to that described for the human moesin FERM-C-terminal tail domain complex.⁴ Dissociation of the FERM and C-terminal tail domains unmask binding sites for other proteins. EBP50 binds to a region of the FERM domain that overlaps with the C-terminal tail,^{20,21} and the ICAM-2 receptor binds to the radixin FERM domain at a site analogous to the first β -strand in the C-terminal tail.²² This site is analogous to where integrin tails anchor to the talin FERM domain,²³ and to where a regulatory intramolecular linker region interacts with the FERM domain of focal adhesion kinase.²⁴ Evidence suggests these states are regulated primarily by the phosphorylation of a threonine residue in the C-terminal domain (equivalent to Thr558 in moesin) and/or the binding of PIP₂.¹ Thr558 lies buried in the FERM-C-terminal tail interface, and its phosphorylation is expected to favor domain dissociation. PIP₂ binds to a site between lobes F1 and F3, and has been proposed to confer subtle conformational changes that favor

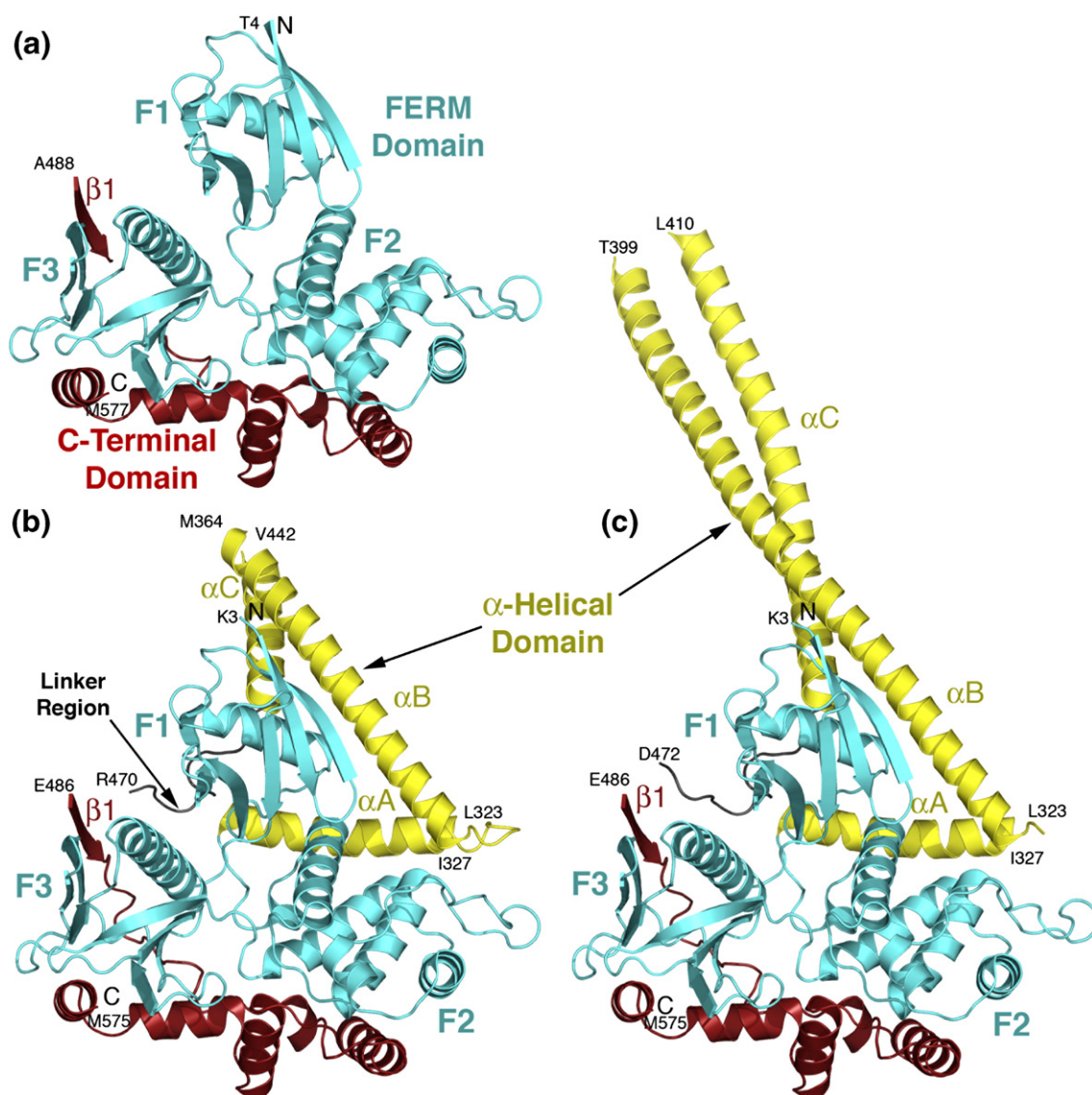


Figure 2. Comparison of dormant human and *Sfmoesin* structures. (a) The human FERM–C-terminal domain complex (PDB code 1EF1). The three lobes of the ERM domain (F1, F2 and F3) are colored cyan and the C-terminal domain is colored red. The $\beta 1$ strand of the C-terminal domain is contributed by a crystal-packing interaction. (b) The 2.1 Å *Sfmoesin* structure. The α -helical domain (yellow) folds into three extended helices (αA , αB and αC), each containing elements that pack against the FERM domain. The αB and αC helices form an anti-parallel coiled-coil. (c) In the 3.0 Å structure, 67 more residues of the ~ 70 Å $\alpha B/\alpha C$ coiled-coil are revealed.

dissociation of the interface, for this site is not obviously masked in the dormant protein.²⁵ Although merlin is expected to have the same domain architecture as ERM proteins,^{4,26} it is activated differently *via* phosphorylation at other sites, and the self-associated, closed form is thought to be responsible for its tumor suppressor activity.²⁷

Here, we report the structure of the full-length, dormant monomeric moesin endogenous to ovarian *Spodoptera frugiperda* cells (*Sfmoesin*), the ERM protein expected to play an essential role in establishing polarity in insect embryos.²⁸ The central α -helical domain is seen to contain three helices, including a striking 70 Å anti-parallel coiled-coil, that form extensive, unanticipated and functionally important interactions with the FERM

domain. We argue that this structure provides a complete and relevant model for the dormant state of ERM proteins, and for what is thought to be the relevant tumor suppressor state of merlin.

Results

Overall structure

Sfmoesin was purified with yields of 0.5 mg/l from ovarian insect cells, and is a stable monomer as determined by gel-filtration chromatography. The cDNA sequence we determined corresponds to a protein of 575 residues, having 83% identity with

Drosophila moesin and ~60% identity with human ERM proteins. The most variability occurs within residues 315–500, which spans most of the α -helical domain and the beginning of the C-terminal tail (Figure 1). Within this region, Sfmoesin and human ERM proteins have <25% sequence identity. Residues 299–461 have significant coiled-coil probability,²⁹ with hydrophobic residues dominating at positions *a* and *d* of the heptad repeat (Figure 1(b)).

We determined two closely related crystal structures of Sfmoesin at 2.1 Å and 3.0 Å resolution (Table 1; Figure 2), with the lower-resolution structure revealing a much larger portion of the α -helical domain. In addition to the expected tri-lobed FERM domain and C-terminal tail interaction, the α -helical domain is revealed to consist of three extended helices (α A, B and C). The first helix folds back under lobe F1, as has been observed in several earlier structures of the open form of ERM-merlin proteins (Figure 3(a)), and is followed by helices that form the outgoing (α B) and incoming (α C) segments of a 70 Å antiparallel coiled-coil. The N terminus of α B (residues 328–350) is not paired with α C, and instead uses the hydrophobic residues of its heptad repeat to interact with a highly-

conserved surface on the F1 lobe (Figures 1(b) and 4). Comparison of the moesin coiled-coil with those from other proteins demonstrates that it has standard geometry, including the N-terminal portion of α B that interacts with F1 (Figure 3).

Although the α B- α C loop of the α -helical domain is not observed, there is sufficient room in the crystal lattice for the missing residues to form a helical hairpin, and there is also no possibility for the formation of a crystalline dimer mediated by the coiled-coil (Figure 5(b)). An examination of *B*-factors shows that the FERM domain is very well ordered, on the whole, as are the segments of the α -helical domain that anchor its α A, α B and α C helices to the F1 lobe (Figure 5(b)). However, *B*-factors for residues in the coiled-coil increase steadily as their distance from the F1 lobe increases, rising to >140 Å² at the termini. Nevertheless, helical electron density for the backbone of these residues is unambiguous. C-terminal to the α C helix (ending with Thr460), a “linker region” threads through the cleft formed between lobes F1 and F3, with residues 461–465 forming a short 3_{10} -helix and residues 465–472 adopting the conformation of a type II polyproline helix. The visible density ends at residue 472, and

Table 1. Crystallographic data and refinement statistics

	A (initial dataset)	B (high-resolution)	C (low-resolution)
<i>A. Data collection</i>			
X-ray source:	ALS 8.3.1	APS 17-ID	APS 19-BM
Wavelength (Å)	1.116	1.000	1.033
Resolution (Å)	3.5	2.1	3.0
Space group	R32	R32	R32
Cell constants			
<i>a</i> = <i>b</i> (Å)	124.1	123.7	126.9
<i>c</i> (Å)	285.0	283.2	272.5
Unique reflections	10,518	43,611	17,202
Redundancy ^a	7.5 (7.6)	4.9 (3.5)	5.4 (5.3)
<i>R</i> _{sym} ^b (%)	22.9 (68.1)	7.9 (33.8)	14.4 (43.7)
Completeness (%)	96.8 (98.1)	88.5 (71.0)	99.3 (99.7)
< <i>I</i> >/< σ _{<i>I</i>} >	7.7 (2.4)	19.7 (3.3)	10.9 (3.3)
<i>B. Refinement statistics</i>			
Resolution (Å)		50–2.1	50–3.0
Total reflections		43,611 (2506) ^c	17202 (1258) ^c
Protein atoms		4004	4507
Non-protein atoms		438	64
r.m.s.d. from ideal			
Bond lengths (Å)		0.010	0.007
Bond angles (deg.)		1.11	0.93
Est. coordinate error (Å)		0.06	0.17
Average <i>B</i> -factor (Å ²)		24.5	35.9
Ramachandran plot			
Most favored regions (%)		96.4	95.4
Disallowed regions (%)		0.2	0.2
<i>R</i> _{work} ^d		17.9 (16.8)	18.1 (26.9)
<i>R</i> _{free} ^e		21.5 (22.9)	24.9 (33.5)
<i>R</i> _{final} ^f		17.6 (16.3)	18.4 (24.7)

^a Numbers in parentheses correspond to the highest resolution shell of data; data set A, 2.74–2.6 Å; data set B, 2.18–2.10 Å; data set C, 3.11–3.00 Å.

^b $R_{\text{sym}} = \sum_{hkl} \sum_i |I(hkl)_i - \bar{I}(hkl)| / \sum_{hkl} I(hkl)_i$, where $I(hkl)$ is the mean intensity of *i* reflections after rejections. A $-1.0 I/\sigma_I$ cutoff was applied to data set C.

^c Numbers in parentheses correspond to the highest resolution shell of data; data set B, 2.15–2.10 Å; data set C, 3.08–3.00 Å.

^d $R_{\text{work}} = \sum_{hkl} ||F_{\text{obs}}(hkl)| - |F_{\text{calc}}(hkl)|| / \sum_{hkl} |F_{\text{obs}}(hkl)|$; no I/σ cutoff was used during refinement.

^e A portion (5%) of the truncated data set was excluded from refinement and used to calculate *R*_{free}.

^f Final *R*-factor after the last rounds of refinement, when all reflections were used.

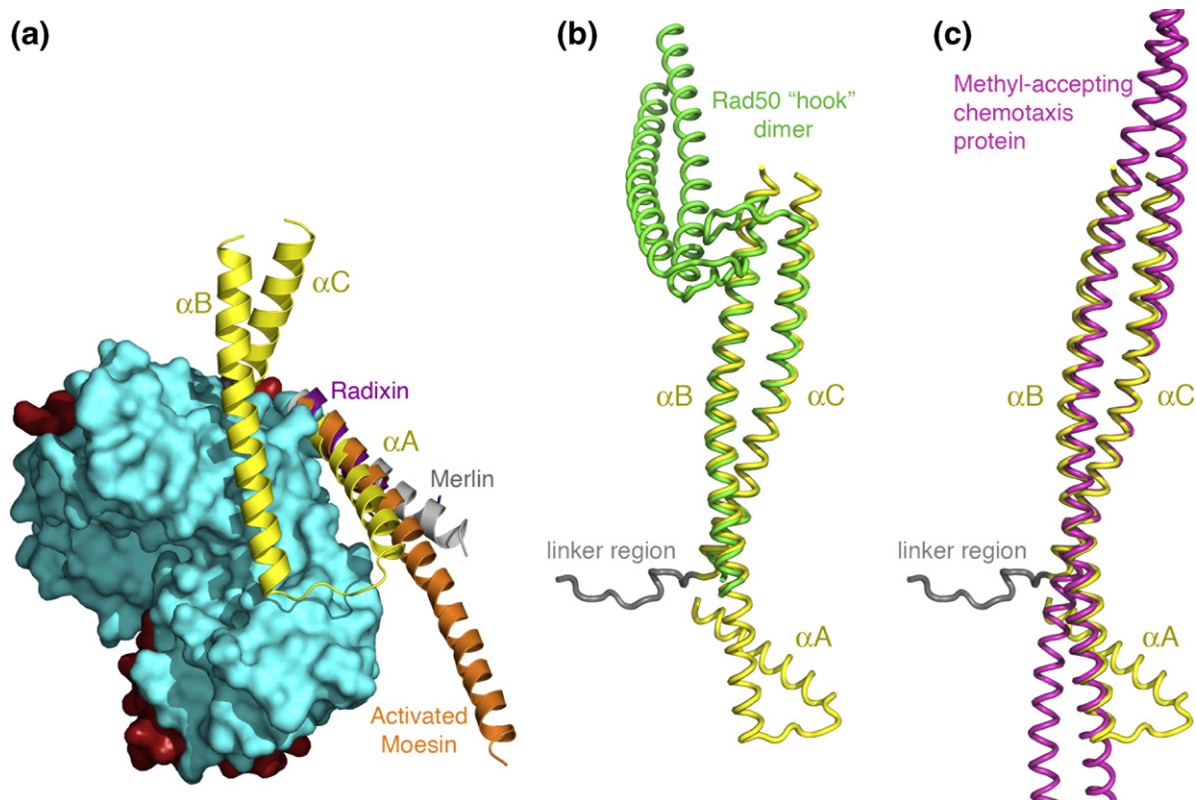


Figure 3. Comparison of the *Sfmoesin* α -helical domain with active ERM domain structures and other coiled-coil domains. (a) The structures of “activated” merlin, radixin, and moesin (PDB entries 1ISN, 1J19, 1E5W, respectively) superimposed on the 2.1 Å structure of *Sfmoesin*, showing that the α A helix does not alter its orientation greatly upon activation. (b) The Rad50 coiled-coil (PDB entry 1L8D) superimposed on that of the 3.0 Å structure of *Sfmoesin* in the same orientation as in (a). In this structure, Rad50 is dimerized through a hook-like structure at the turn of the coiled-coil.⁴⁸ (c) Superposition of the methyl-accepting chemotaxis protein coiled-coil (PDB entry 2CH7).⁴⁹ This coiled-coil is half of an antiparallel four-helix bundle. Note that the N-terminal segment of *Sfmoesin* α B, which does not participate in a coiled-coil with α A, maintains proper coiled-coil geometry. Superpositions are the optimal fits reported by a search of the PDB using the DALI server.⁵⁰

begins again at Glu486, the first residue of a β -strand associated with lobe F3 that defines the start of the C-terminal tail domain. The intervening disordered loop is enriched with acidic residues in ERM proteins (Figure 1(b)).

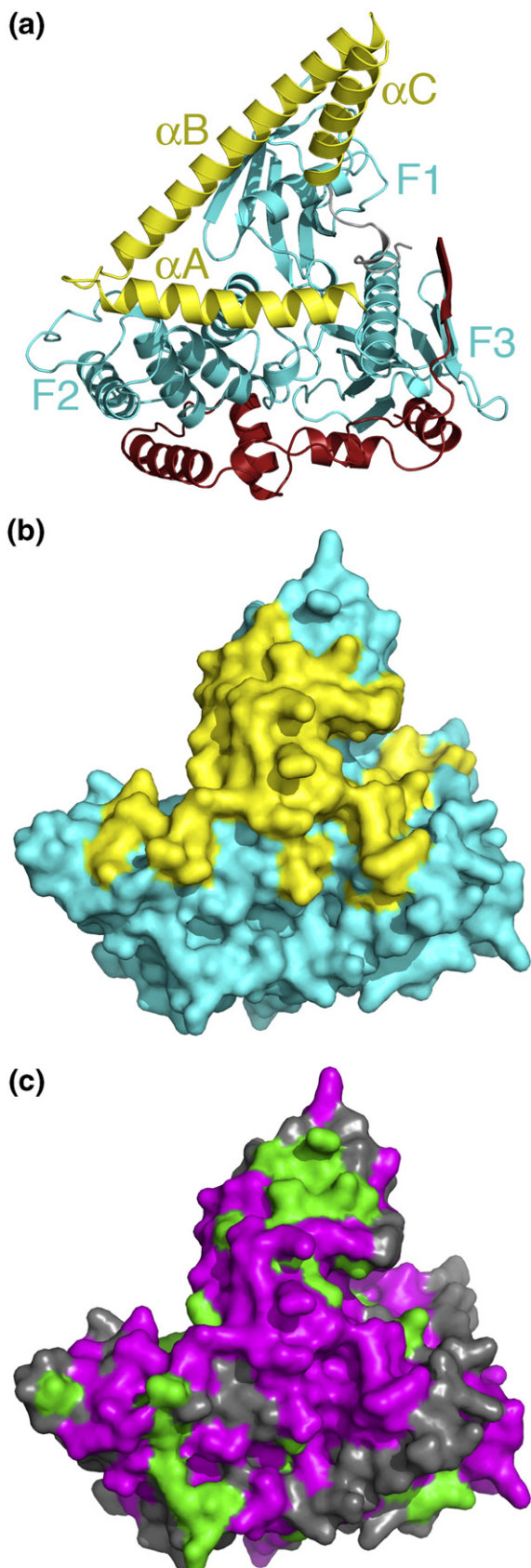
Interactions of the α -helical domain with the FERM domain

The central α -helical domain of moesin forms multiple, extensive contacts with highly conserved surfaces of the FERM domain (Figure 4). One surface, formed by both the F1 and F2 lobes, interacts with the α A helix, and two other faces of F1 stabilize and give direction to the α B/ α C coiled-coil: one face interacts with the N-terminal portion of α B and the other provides a specific docking site for the residues at and after the C-terminal end of helix α C. We refer to these two interaction surfaces as the launching and landing pads for the antiparallel coiled-coil, respectively. The contacts that the α -helical domain and the subsequent linker region (Figure 1) form with the FERM domain bury 3800 Å² of total accessible surface area.

The interactions of α A are bipartite (Figure 6(a)). The highly conserved N terminus of α A (residues 298–313) forms extensive hydrophobic interactions with a continuous surface of F1 and F2, wherein the side-chain of Ile94 (in F2) is buried in a hydrophobic pocket formed by Val302, Met305, Lys306 and Ala 309 (in α A), while the side-chain of Met305 (α A) is buried in a pocket formed by Arg40 and Trp43 (in F1) and His465 (linker region). In the second interaction region, the C terminus of α A and the subsequent α A- α B loop form primarily electrostatic contacts with F2. The basic side-chains of Arg184, Lys316, Arg320, Arg332 (all invariant or highly conserved) cluster together, and are in close proximity to the acidic side-chains of Glu96, Glu185 and Glu326 (also highly conserved). The backbone of the α A- α B loop is disordered in the 3.0 Å structure (Figure 5(b)), and has relatively high *B*-factors in the 2.1 Å structure, suggesting marginal stability of these interactions.

The launching pad interaction for the α B/ α C coiled-coil is formed by the hydrophobic face of the α B helix just before the coiled-coil, which abuts the α A helix of the F1 lobe (Figure 6(b)). The highly conserved residues that make up this surface,

Tyr340, Leu344 and Met347, occupy the *d-a-d* positions of the coiled-coil heptad repeat. Specific hydrogen bonds are formed between the side-chain of Gln337 (α B) and the backbone of Glu15 (F1), the



side-chain of Arg343 with backbone carbonyl groups of residues 35 and 36, and the Tyr340 hydroxyl group with the side-chain of Asp13.

The landing pad interactions involve both the end of the α C helix and the linker region (Figure 6(c)). The amino group of Lys35, conserved as either Lys or Arg among ERM-merlin proteins, caps the end of the α C helix. Lys27 and Asp31, which form an invariant salt-bridge within F1, coordinate the buried hydroxyl group of Thr461. His465 forms a hydrogen bond with the side-chain of Asp301 in the first turn of the α A helix, joining the two ends of the α -helical domain. The side-chain of His466 packs in a conserved hydrophobic pocket formed by Lys27, Phe30, Val42 and Leu61. Subsequently, the side-chain of Val467 packs against F3, and Glu469 forms two hydrogen bonds with the backbone nitrogen atoms of residues 61 and 62. Invariant moesin residues Glu289 and Arg293 (F3) together form a salt-bridge as well as three hydrogen bonds with the backbone of residues 465, 466 and 468.

Comparisons with previous ERM structures

Earlier structures of truncated/activated ERM proteins have included only the first 49, 27 and 14 residues of the α -helical domain (Figure 3(a)). The intact *Sfmoesin* α A helix stays more tightly associated with the FERM domain than the others, possibly because they are missing subsequent residues that, as in *Sfmoesin*, would help restrain the C-terminal end of this helix.

Overlay of *Sfmoesin* with the radixin-IP₃ complex demonstrates that the IP₃ binding site is sterically blocked by the linker region (Figure 7). Moreover, the disordered loop joining the linker region to the C-terminal tail is intensely acidic in ERM proteins (Figure 1(b)). Thus, the linker and subsequent loop dramatically lower the electrostatic potential of a surface of the FERM domain (Figure 7(b) and (c)) believed to associate with negatively charged membranes in the active form of ERM proteins. Because the 2 h soak of IP₃ into the *Sfmoesin* crystals used for the low-resolution data set showed no electron density for this ligand, IP₃ alone under the crystal-harvesting conditions is insufficient to displace the linker and subsequent loop, rendering them an effective mask for PIP₂ binding. This appears to conflict with a recent report that PIP₂ binding is a prerequisite for C-terminal domain

Figure 4. Extent and sequence conservation of the surfaces buried by the α -helical domain and linker region. (a) The *Sfmoesin* FERM domain. The view is rotated by $\sim 180^\circ$ around a vertical axis from that in Figure 2. (b) Molecular surface of the FERM domain. Yellow regions are those in contact with the α -helical domain and linker region ($\sim 1800 \text{ \AA}^2$ of buried accessible surface area). (c) Conservation of the FERM domain. Magenta regions correspond to residues that are either identical or substituted conservatively (e.g. Asp/Glu, Arg/Lys, Ser/Thr) in all ERM-merlin proteins. Green regions correspond to residues conserved only in the ERM family.

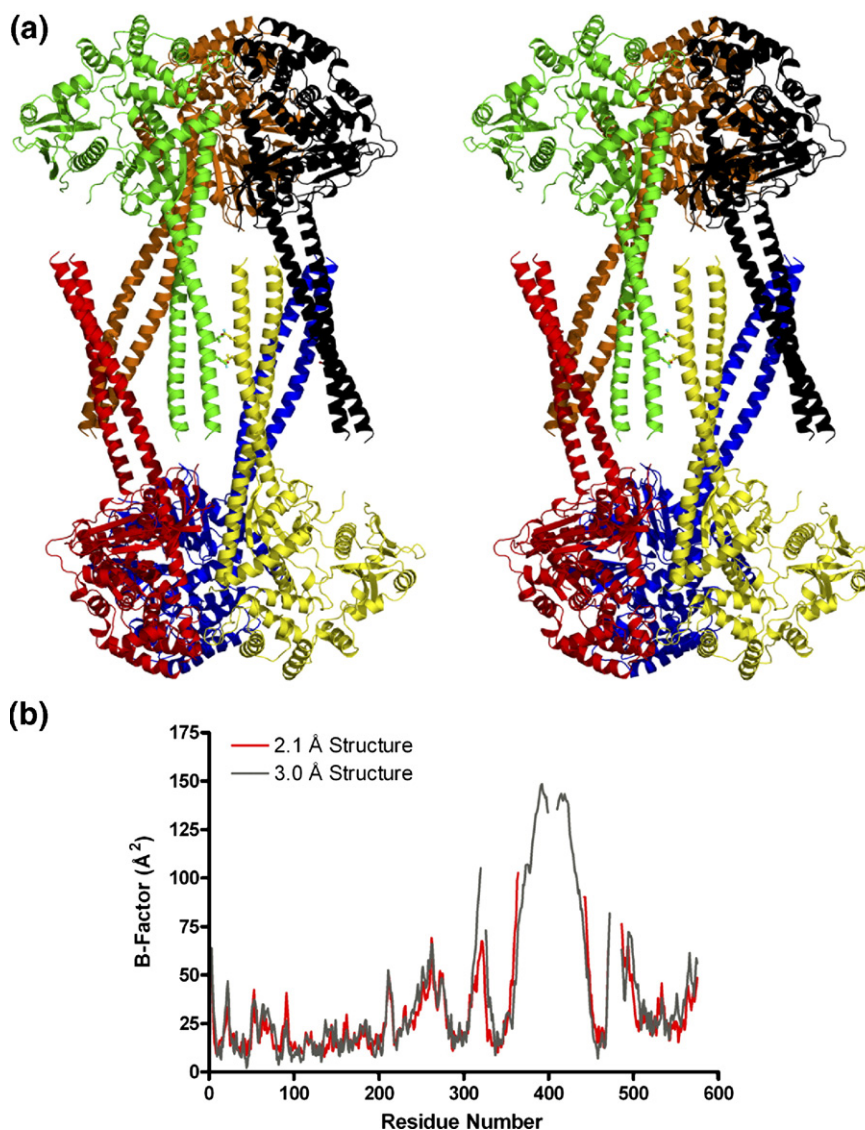


Figure 5. Crystal packing interactions and mobility of the α -helical domain. (a) Stereo view along the crystallographic 2-fold axis of a D_3 center in the crystals of the 3.0 Å structure. Each asymmetric unit in the cluster is colored uniquely. In this structure, differences in lattice packing tilt the $\alpha B/\alpha C$ coiled-coil region by 7° with respect to the 2.1 Å structure, allowing it to form crystal contacts with a 2-fold-related coiled-coil *via* the side-chains of Gln426 and Leu430 (ball-and-stick models). Only residues 400–409 are missing from its helical turn. This structure eliminates the possibility of a dimer mediated by the coiled-coil in the crystalline lattice. (b) Temperature factors as a function of residue position in the 2.1 Å and 3.0 Å structures of *Sfmoesin*. The regions of the α -helical domain that contact the FERM domains are as stable as the FERM domain, while those at greater distances from the ERM domain have gradually increasing mobility. The change in crystal contacts between the two structures orders more of the $\alpha B/\alpha C$ coiled-coil in the low-resolution structure, and disorders part of the αA - αB loop (residues 312–325).

phosphorylation in ezrin.³⁰ However, IP_3 may be a poor mimic for PIP_2 in the context of a phospholipid bilayer.

Finally, the *Sfmoesin* structure confirms the structure and register of the $\beta 1$ strand in the C-terminal tail (Figures 1, 2(b) and 7(a) and (b)), which is domain-

Figure 6. Stereo views of interdomain contacts of the *Sfmoesin* α -helical domain and linker region. (a) The αA helix (yellow) interacts with the F1 and F2 lobes (cyan) in a bipartite fashion. Carbon atoms are shown with the same color as the backbone: oxygen, red; nitrogen, blue; and sulfur, green. Specific hydrogen bonds are shown as broken black lines. Residues colored with white carbon atoms indicate side-chains that are disordered or exist in multiple conformations in the 2.1 Å crystal structure. (b) The launching pad involves the hydrophobic face of αB and a highly conserved surface of the F1 lobe. Met347 is analogous to the site of tyrosine phosphorylation in ezrin,^{35,36} which leads to activation of ezrin in response to growth factor stimulation. Mutation of the residue analogous to Leu344 to proline in merlin is associated with NF2.³⁹ Both modifications in the context of the *Sfmoesin* structure likely disrupt this interface. (c) The landing pad is formed by the end of the αC helix and the linker region. Contacts between the linker region and the F1 lobe are dominated by backbone-side-chain interactions, possibly explaining the lack of strong sequence conservation in this region of the α -helical domain. Mutation of the residue analogous to Trp43 and residues in the F1 αA helix in merlin are also associated with NF2.^{39,51} These changes likely disrupt the observed interdomain contacts.

swapped in the human moesin FERM/C-terminal domain complex and masks the ICAM-2 peptide binding site observed in the radixin-ICAM-2

complex.²² The intact path of this strand to the remainder of the C-terminal domain is therefore fully defined in *Sf*moesin. Sequence comparison suggests

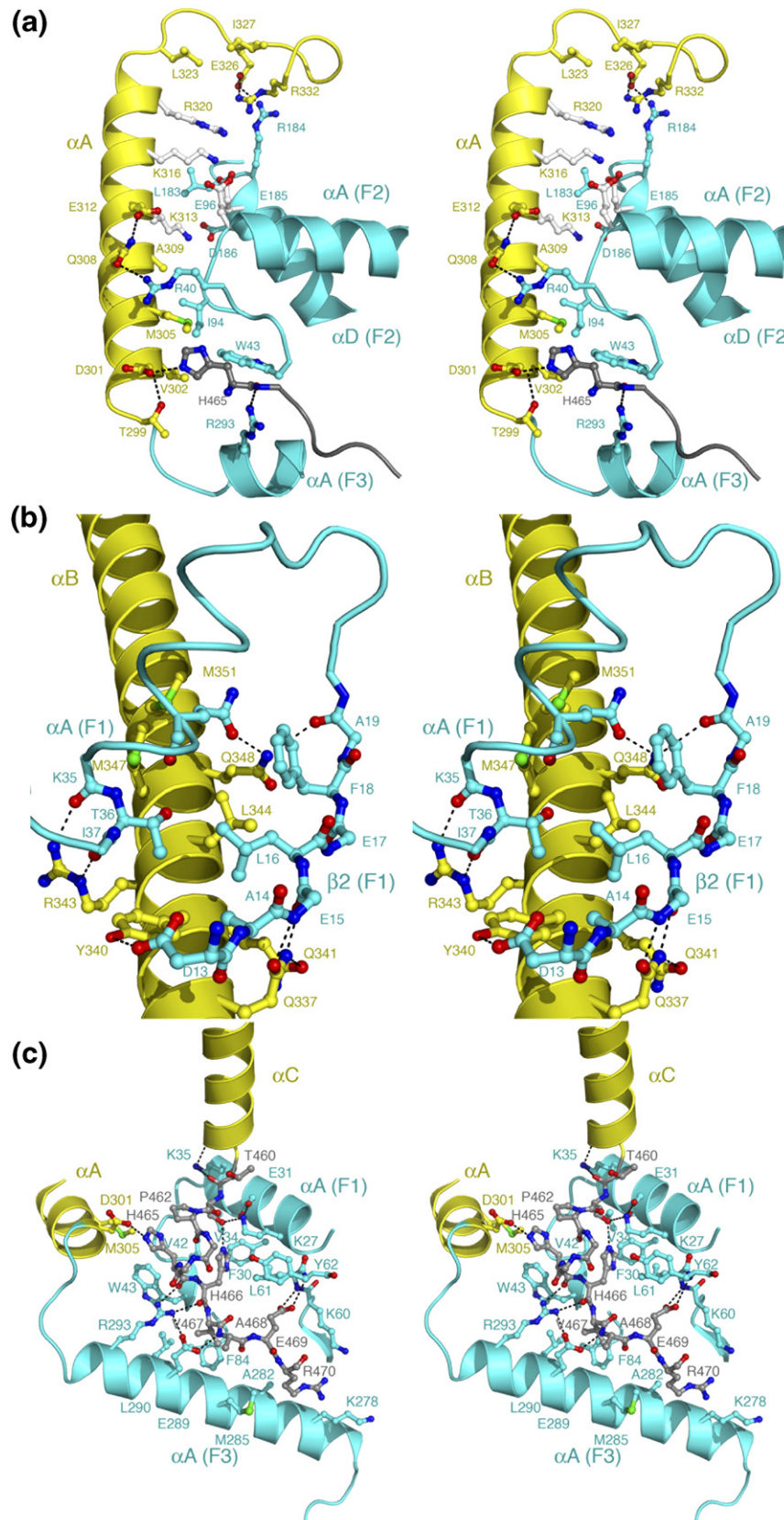


Figure 6 (legend on opposite page)

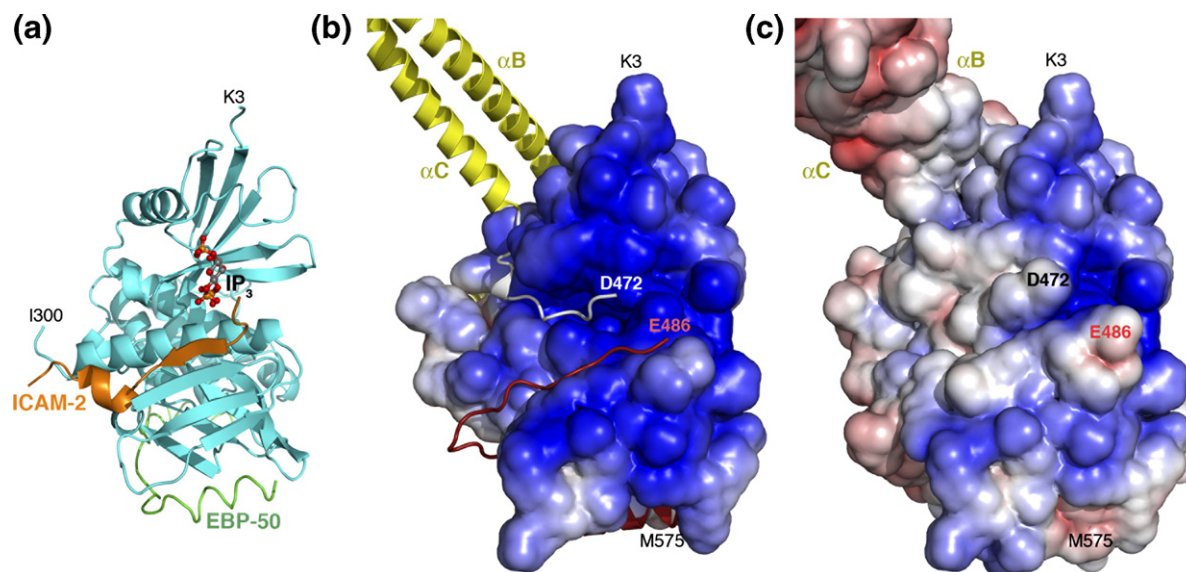


Figure 7. The known intermolecular binding sites of ERM proteins are masked in the dormant structure. (a) The ICAM-2 (orange cartoon), IP₃ (ball-and-sticks), and EBP50 (green coil) ligands mapped onto the structure of *Sfmoesin* (from PDB entries 1J19, 1GC6 and 1SGH, respectively). (b) Solvent-accessible surface of the FERM domain of *Sfmoesin* with the α -helical domain and C-terminal domain superimposed. The surface is oriented as in (a) and colored by its electrostatic potential, contoured from -6.0 (red) to $+6.0$ kT/e⁻ (blue). This intensely basic surface likely helps moesin to bind negatively charged lipid bilayers, such as those that contain PIP₂ (see (a)). (c) The electrostatic surface of dormant *Sfmoesin*. The association of the α -helical domain and the linker region ablates the positive charge of the surface and masks the PIP₂ site. The ICAM-2 peptide binding site is masked by the β 1-strand of the C-terminal domain. The electrostatic calculation does not take into account the negatively charged, disordered loop (residues 473–485) that connects the linker to the C-terminal domain.

that all ERM-merlin proteins will share an analogous β -strand interaction with the F3 domain (Figure 1(b)).

Discussion

A model relevant to the entire ERM-merlin family

The structure of the endogenous, intact *Sfmoesin* reported here provides a very important advance in the study of ERM proteins, as it defines the complete dormant state of these proteins. For merlin, it has been postulated that the analogous closed conformation is responsible for tumor suppressor activity.²⁷ In this conformation, the *Sfmoesin* structure demonstrates that there are extensive interactions of the central α -helical domain with the FERM domain, indicating that the α -helical domain plays a surprisingly active role in masking additional ligand-binding and activation sites.

Conservation in other ERM-merlin proteins of the arrangement of the *Sfmoesin* α A, α B and α C helices in the α -helical domain is supported strongly by sequence conservation and biochemical studies. Unlike the α A helix, the coiled-coil portion of α B and α C (but not the α A- α B or α B- α C loops) has an almost perfect heptad repeat. Our structure also easily accommodates the seven residue insertion found in human radixin, ezrin and merlin proteins within or near the α A- α B loop (Figure 1(b)). In addition, limited proteolysis of the recombinant isolated α -helical

domain of human radixin show rapid cleavage at residue 330 followed by cleavage at residue 351 to yield a relatively stable fragment spanning residues 352–469.¹⁷ The first cleavage site corresponds to the highly mobile α A- α B loop (Figure 4(b)) and the second matches the position within α B just before the start of the coiled-coil segment. The stable proteolytic fragment is thus a reasonable match with the α B/ α C coiled-coil region of the *Sfmoesin* structure (Figure 1(b)). This correlation leads to the rather remarkable inference that, even in the absence of contacts with the FERM domain, there are features intrinsic to the α -helical domain that partition it into the three distinct helices observed in the *Sfmoesin* structure.

Surfaces of the FERM domain that contact the α -helical domain are remarkably well conserved (Figure 4), supporting a biological role for these interactions. Interdomain contacts include the docking of α A onto the FERM domain *via* Met305, Lys306 and Ala 309 (Figure 6(a)), as observed in earlier crystal structures of activated ERM-merlin proteins (Figure 3(a)). The N terminus of α B from the α -helical domain interacts with a nearly invariant surface of the F1 lobe with no previously ascribed function. The helical domain α C helix is followed by a stop signal (T/STPxxxxxE) conserved among moesin proteins that also contains two residues (the second Thr and the ultimate Glu) that form specific interactions with lobe F1 (Figure 6(c)). Although ezrin, radixin and merlin have a polyproline stretch in this region (Figure 1(b)), this is nevertheless

compatible with the salient features of the *Sfmoesin* linker region. Specifically, the most important interactions made by the “spacer” residues (given as ‘x’ above) as they wind toward the IP₃ binding site are made primarily by their main-chain atoms (Figure 6(c)). In addition, the backbone conformation of the linker is superimposable with a polyproline helix. Finally, it seems likely that the conserved, highly acidic region joining the linker region and the C-terminal domain (Figure 1(b)) in ERM proteins could play a functional role in hindering PIP₂ and membrane interactions until the α -helical and/or C-terminal domains become displaced.

The α -helical domain in activated ERM-merlin proteins

Biochemical studies of ERM-merlin proteins and the *Sfmoesin* structure now support the idea that the α -helical domain can adopt a variety of physiologically relevant conformations, ranging from the relatively condensed, inactive structure that we observe in *Sfmoesin*, to a relatively protected one in which the domain is dissociated from the FERM domain yet forms two or three helices that retain the observed α B/ α C coiled-coil interaction, to a fully extended helix. The existence of the latter two states is supported by limited proteolytic digestion and biophysical studies of the isolated α -helical domain of radixin, and the activated structure of moesin.^{17,31}

For full activation of ERM proteins, large conformational changes are needed to expose various regulatory sites, including that for PIP₂, which is masked by the linker region (Figure 7). This direct model for activation is in contrast to a previous model, wherein it was speculated that PIP₂ binding led to activation *via* relatively subtle conformational changes.²⁵ Unraveling the α B/ α C coiled-coil observed in the dormant state also appears to be a prerequisite for gaining access to the buried hydrophobic residues that compose the A-kinase anchoring sites reported for ezrin and merlin.^{32,33} Consistent with this, binding of merlin to RI β occurs only in forms of merlin that mimic the open state (e.g., C-terminally truncated). Thus, the putative “switchblade-like” opening of the α B/ α C coiled-coil into an extended helix may represent yet another functionally relevant unmasking event. The interconversion of helical and non-helical regions required for the proposed switchblade-like opening of the helical domain has good precedent, such as the pH-triggered conformational change observed in hemagglutinin-mediated membrane fusion.³⁴ Conversion of the α B/ α C coiled-coil to a fully extended state upon activation is supported also by biophysical studies of the isolated helical domain of radixin in which this region appears to form an unusual monomeric 240 Å long helix.¹⁷ This seems possible, given the strong helical potential of the α A- α B and α B- α C loops (Figure 1(b)) and the fact that the 50 residues of the α -helical domain present in an activated moesin FERM structure continue as an uninter-

rupted helix that leaves the FERM domain in the direction of α A,³¹ rather than breaking at the α A- α B turn, as is observed in *Sfmoesin* (Figure 3(a)). Conversion to this extended form is likely to be stabilized by ligands that favor binding to a single amphipathic helix, such as AKAPs.

Until now there has been no concrete model for how Tyr353 phosphorylation of ezrin contributes to its activation.^{35,36} The structurally equivalent residue in *Sfmoesin* (Met347) is buried at the end of the launching pad of α B (Figure 6(b)) and it is reasonable to assume that Tyr353 in ezrin interacts similarly. Phosphorylation of Tyr353 in ezrin would be expected to strongly favor release of the α -helical domain from the FERM domain.

Finally, our studies provide insight into the structures of the dormant ERM homodimers that, when compared to dormant monomers, have indistinguishable patterns of limited proteolysis.³⁷ We propose that in these dimers, the α B- α C turn does not exist, and instead two molecules associate *via* a fully-extended α B and α C helix that forms an intermolecular antiparallel coiled-coil and allows the C-terminal tail domain of each chain to interact with the FERM domain of the other chain. In this way, exactly the same launching and landing pad contacts would be maintained. Consistent with this model, the α B- α C turn consists of exactly seven residues (Figure 1(b)), so that the heptad repeat would be perfectly maintained in such a domain-swapped dimer. While the physiological relevance of dormant homodimers is unknown, this structural arrangement could be present in the ezrin-merlin (and other) heterodimers that likely do exist *in vivo*.³⁸

An explanation for enigmatic mutations in the tumor suppressor merlin

Many of the missense mutations associated with NF2^{27,39} defied explanation when mapped onto earlier atomic structures of ERM-merlin proteins. When mapped on the tertiary structure of *Sfmoesin* (Figure 1(b)), the structural impact of many of these merlin mutations becomes clear, lending further support to the biological relevance of the α -helical domain contacts. Of the non-truncating mutations of merlin that are known to be pathogenic in cells, 16 are found in the F1 lobe, nine in F2, six in F3, ten in the α -helical domain and seven in the C-terminal domain. Of those that are purely missense (not insertions or deletions), ten are in F1, four are in F2, four are in F3, ten are in the α -helical domain, and six are in the C-terminal tail. The preponderance of disruptions in the F1 lobe and the α -helical domain implies an important role for these domains in maintaining merlin in a stable, closed, active form. The F1 lobe α A helix, straddled by the α B and α C helices of the α -helical domain (Figure 6), is particularly rich in NF2-associated disruptions. Also, the F1 lobe α A- β 3 loop, with residues interacting with both the α A helix and the landing pad, is relatively rich in mutations. Mutations

identified in the α -helical domain of merlin are dispersed throughout, but some are found in the highly conserved N terminus of α A: at Leu323 (L339F in merlin), a residue that helps to stabilize the α A- α B loop (Figure 6(a)), and at Leu344 (L360P), a buried α B residue in the launching pad interface (Figure 6(b)). This remarkable correlation between sites of disease-causing merlin mutations and sites involved in stabilizing interactions between the α -helical and FERM domains supports the conclusion that the closed form of merlin is required for its tumor suppressor activity.

An active regulatory role for the α -helical domain

The crystal structure of the FERM-C-terminal tail domain complex of human moesin showed that the complex is held together by five, largely independent, interacting parts.⁴ We can now extend this model to include the launching and landing pads of the central α -helical domain, which together with the coiled-coil interaction provide the sixth, seventh and eighth points of interaction that can be modulated independently to influence the net affinity of the masking interactions. Interestingly, these interaction points with the FERM domain are, apparently, purposefully of lower affinity than they could be. For example, ICAM and EBP50 peptides have conserved sequence features not present in the ERM sequences, and they bind to their respective sites on the FERM domain much more tightly *in trans* (nanomolar affinities) than does the tail domain *in cis*. Such distributed binding involving many purposefully medium or low-affinity interactions creates a net high-affinity interaction *via* the chelate effect,⁴⁰ but that can, in principle, have its affinity fine-tuned to many different levels by a wide variety of effectors. In addition to the known effectors discussed above, the interactions of the α -helical domain allow speculation that another modulator of activation could be the binding of SH3 domains to the polyproline sequences that fill the F1-F3 cleft in ezrin, radixin and merlin. In accordance with this idea, the focal adhesion kinase FERM domain, although distantly related to ERM proteins and lacking an α -helical domain, has a regulatory linker region C-terminal to the FERM domain that occupies the cleft between its F1 and F3 lobes. The linker forms a β -strand interaction, analogous to but opposite in orientation to the β 1 strand of the *Sf*moesin C-terminal domain, and a polyproline helix, bound to F3, that can be sequestered by the SH3 domain of Src.²⁴

We conclude that the central α -helical domain is not just a passive structural feature that is important for facilitating effective cytoskeletal-membrane linkage once the activated proteins are generated. Instead, it is actively involved in masking, burying $\sim 2000 \text{ \AA}^2$ of FERM domain surface area, about 75% of that buried by the C-terminal tail interaction. Together, the central and C-terminal tail domains bury 4700 \AA^2 , which is 25% of the accessible surface area of the FERM domain and mask directly all known sites for

activating ligands or modifications (i.e. the PIP₂ binding site and phosphorylation sites Thr558 or ezrin Tyr353) or docking targets (EBP50/NHERF, ICAM and actin). As alluded to before,⁴ and extended here from five to eight points of interaction, we propose that ERM proteins are subject to a rheostat-like mechanism for a graded regulation of activation. Multiple regulatory pathways that impinge on the ERM proteins could be combined and/or integrated to allow for different levels of release of the coiled-coil domain, depending on their sites of interaction, and hence unmasking of ligand-binding sites. Finally, our studies have now yielded an important image that fully describes the structural components involved in the closed form of ERM-merlin proteins. Such information will be exceptionally useful in the design and interpretation of a new generation of experiments aimed at unraveling the activation mechanisms of ERM proteins and to better understand the tumor suppression mechanism of merlin.

Materials and Methods

Purification

The endogenous moesin protein from *Sf* ovarian cells was purified by the protocol used to purify G protein-coupled receptor kinase 2 (GRK2).⁴¹ Except in the first purification, wherein *Sf*moesin was mistakenly purified instead of GRK2, *Sf*moesin-containing fractions were identified by Western analysis using a rabbit polyclonal antibody (a gift from D. Kiehart, Duke University) at a 1:40,000 dilution. The final purification step was over two tandem S200 gel-filtration columns (Amersham Pharmacia Biotech) equilibrated in 20 mM Hepes (pH 7.8–8.0), 200 mM NaCl, 2 mM DTT. The protein eluted with an expected molecular mass of 74 kDa based on comparison with Bio-Rad gel filtration standards. The resulting homogeneous moesin was concentrated to 4.75 mg/ml. The total yield was 0.12–0.45 mg/1 of *Sf* cell culture.

Crystallization

*Sf*moesin crystals were grown by the hanging-drop, vapor-diffusion method using the conditions used for GRK2,⁴² with 100 mM Hepes (pH 7.8) as the buffer for the well solution. For harvesting, cryoprotectant solution (25% (v/v) PEG400, 15% (w/v) PEG 8K, 50 mM phosphoserine (pH 7.5), 800 mM NaCl, 800 mM urea, 1 mM DTT, 22 mM Hepes (pH 8.0) and 22 mM Hepes, pH 7.8) was added 1 μ l at a time into the hanging drop, and then crystals were transferred into 100% cryoprotectant solution. The crystals were then flash-frozen in liquid nitrogen on nylon loops (Hampton Research).

Diffraction data collection

A preliminary 3.5 \AA data set (data set A) was collected at the Advanced Light Source (ALS) on a Quantum 210 CCD detector (ADSC) at beam-line 8.3.1 and was used for the initial structure determination. A higher resolution data set (data set B) was later collected at the Advanced Photon Source (APS) on a Quantum 4 CCD detector (ADSC) at

beam-line 17-ID. Lastly, a 3.0 Å data set (data set C) was collected at APS beam-line 19-BM from a crystal soaked for 2 h in harvesting solution supplemented with 1 mM IP_3 . Data were indexed, integrated and scaled using HKL2000.⁴³ The crystal soaked in IP_3 had significantly different cell constants (>1% change), suggesting a conformational change. Unit cell parameters and data collection statistics are summarized in Table 1.

Identification of moesin by mass spectrometry

Sfmoesin was purified using the scheme used for GRK2, had a similar apparent molecular mass (74 kDa for *Sfmoesin*, 80 kDa for GRK2) and crystallized under conditions identical with those used for GRK2. However, molecular replacement using the structure of GRK2 failed to yield a solution. To verify the identity of the crystallized protein, a drop of the protein solution (roughly 5 µg) was taken from the hanging drops used for crystallization, subjected to SDS-PAGE (10% polyacrylamide gel), and then subjected to trypsin digestion in-gel followed by matrix-assisted laser desorption/ionization mass spectrometry at the Institute for Cellular and Molecular Biology Protein Core Facility (UT Austin). Four abundant peptide peaks were generated, and their resulting masses were best matched to *Drosophila melanogaster* moesin (residues 29–36, QLFDQVVK; 42–54, EVWFFGLQYTDSK; 195–210, IAQDLEMYGVNYFEIR; and 239–247, IGFPWSEIR), suggesting that the crystallized protein was in fact the moesin protein endogenous to *S. fergusonii*, which had not been sequenced.

Structure determination and refinement

Phases were determined by straightforward molecular replacement using the structure of the FERM/C-terminal tail complex of human moesin (PDB code 1EF1) as a search model, reflections from data set A and the program PHASER from the CCP4 suite.⁴⁴ The resulting model was refined with simulated annealing in CNS,⁴⁵ and then REFMAC5.⁴⁶ The sequence of *D. melanogaster* moesin was used for initial model building. The high resolution of data set B permitted "sequencing by electron density" in the best-resolved regions, and refinement was continued in REFMAC5. Upon sequencing of the *Sfmoesin* cDNA (see below), the refinement was completed (Table 1). At an R -factor of 17.9%, and R_{free} of 21.5%, the use of R_{free} was discontinued so that all reflections could be used during the last few rounds of refinement. The final model for data set B contains residues 3–364, 442–470 and 486–575 (out of 575 total) and has R_{final} = 16.3%. Difference Fourier analysis between data sets B and C revealed no significant electron density that might correspond to IP_3 , which was soaked into the crystals used for data set C. However, these maps revealed that significantly more of the α -helical domain was ordered in data set C, and so an atomic model was refined using this data set as well. The final model from data set C contains residues 3–320, 326–399, 410–472, and 486–575. The different unit cell constants for data set C (Table 1) presumably derive from the 2 h soak in harvesting solution (as compared to several minutes for data set B). In the 3.0 Å structure, changes in crystal contacts disorder the α A- α B loop (residues 312–325) and lead to the formation of a new crystal contact stabilizing the α B/ α C coiled-coil (Figure 5(a)). In both structures, the backbone of residue 252 is in a disallowed region of the Ramachandran plot (Table 1). This residue, conserved as Asp or Glu in all ERM-merlin proteins, is in the $i+1$

position of a type II' β -turn (normally occupied by glycine), has good electron density, and the analogous residue in other ERM structures has the same conformation. The backbone nitrogen atom of Asp²⁵² forms a hydrogen bond with residue 486, the first visible residue of β 1 in the C-terminal tail domain.

Sequencing of *Sfmoesin*

To determine the sequence of *Sfmoesin*, a portion of the highly conserved FERM domain was amplified using PCR with degenerate oligonucleotide primers followed by 5' and 3' RACE to complete the flanking sequences. Total RNA was isolated from *Sf9* cell cultures using Trizol (Invitrogen). First-strand synthesis was performed using random hexamer primers and Multiscribe (Applied Biosystems) reverse transcriptase. Using this template DNA, PCR was performed using degenerate primers previously described for cloning of *D. melanogaster* moesin,⁴⁷ as well as degenerate primers based on the *Sfmoesin* protein sequence determined by mass spectrometry. Once the sequence of the FERM domain was obtained, 5' and 3' RACE were performed to obtain flanking sequences using the GeneRacer system (Invitrogen) following the manufacturer's instructions.

Protein Data Bank accession numbers

Coordinates and intensities corresponding to data sets B and C are deposited with the Protein Data Bank under the accession numbers 2IIJ and 2IIK, respectively.

The sequence of *Sfmoesin* is available as Genbank entry EF071985.

Acknowledgements

We thank D. Lodowski (UT Austin), Ingo Focken and Jochen Huber (Sanofi-Aventis Deutschland GmbH) for technical assistance. Support was provided by American Heart Association Scientist Development grant 0235273N, NIH grant HL071818, American Cancer Society Research Scholar grant 04-185-01 (to J.J.G.T.), NIH grant NS034783 (to R.G.F.), and NIH grant GM36652 (to A.P.B.). The Advanced Light Source (ALS) is supported by the Director, Office of Science, Office of Basic Energy Sciences, Materials Sciences Division, of the U.S. Department of Energy under Contract no. DE-AC03-76SF00098 at Lawrence Berkeley National Laboratory. Beam-line 17-ID of the Industrial Macromolecular Crystallography Association Collaborative Access Team (IMCA-CAT) at the Advanced Photon Source (Argonne, IL) is supported by the companies of the Industrial Macromolecular Crystallography Association through a contract with Illinois Institute of Technology (IIT), executed through the IIT Center for Synchrotron Radiation Research and Instrumentation. Use of the Argonne National Laboratory Structural Biology Center beamlines at the Advanced Photon Source was supported by the U. S. Department of Energy, Office of Biological and Environmental Research, under Contract no. W-31-109-ENG-38.

References

- Bretscher, A., Edwards, K. & Fehon, R. G. (2002). ERM proteins and merlin: integrators at the cell cortex. *Nature Rev. Cell Mol. Biol.* **3**, 586–599.
- Polesello, C. & Payre, F. (2004). Small is beautiful: what flies tell us about ERM protein function in development. *Trends Cell Biol.* **14**, 294–302.
- Chishti, A. H., Kim, A. C., Marfatia, S. M., Lutchman, M., Hanspal, M., Jindal, H. *et al.* (1998). The FERM domain: a unique module involved in the linkage of cytoplasmic proteins to the membrane. *Trends Biochem. Sci.* **23**, 281–282.
- Pearson, M. A., Reczek, D., Bretscher, A. & Karplus, P. A. (2000). Structure of the ERM protein moesin reveals the FERM domain fold masked by an extended actin binding tail domain. *Cell*, **101**, 259–270.
- Morrison, H., Sherman, L. S., Legg, J., Banine, F., Isacke, C., Haipek, C. A. *et al.* (2001). The NF2 tumor suppressor gene product, merlin, mediates contact inhibition of growth through interactions with CD44. *Genes Dev.* **15**, 968–980.
- Yonemura, S., Hirao, M., Doi, Y., Takahashi, N., Kondo, T., Tsukita, S. & Tsukita, S. (1998). Ezrin/radixin/moesin (ERM) proteins bind to a positively charged amino acid cluster in the juxta-membrane cytoplasmic domain of CD44, CD43, and ICAM-2. *J. Cell Biol.* **140**, 885–895.
- Heiska, L., Alftan, K., Gronholm, M., Vilja, P., Vaehri, A. & Carpen, O. (1998). Association of ezrin with intercellular adhesion molecule-1 and -2 (ICAM-1 and ICAM-2). Regulation by phosphatidylinositol 4,5-bisphosphate. *J. Biol. Chem.* **273**, 21893–21900.
- Helander, T. S., Carpen, O., Turunen, O., Kovanen, P. E., Vaehri, A. & Timonen, T. (1996). ICAM-2 redistributed by ezrin as a target for killer cells. *Nature*, **382**, 265–268.
- Tsukita, S., Oishi, K., Sato, N., Sagara, J., Kawai, A. & Tsukita, S. (1994). ERM family members as molecular linkers between the cell surface glycoprotein CD44 and actin-based cytoskeletons. *J. Cell Biol.* **126**, 391–401.
- Reczek, D., Berryman, M. & Bretscher, A. (1997). Identification of EBP50: A PDZ-containing phosphoprotein that associates with members of the ezrin-radixin-moesin family. *J. Cell Biol.* **139**, 169–179.
- Reczek, D. & Bretscher, A. (1998). The carboxyl-terminal region of EBP50 binds to a site in the amino-terminal domain of ezrin that is masked in the dormant molecule. *J. Biol. Chem.* **273**, 18452–18458.
- Murthy, A., Gonzalez-Agosti, C., Cordero, E., Pinney, D., Candia, C., Solomon, F. *et al.* (1998). NHE-RF, a regulatory cofactor for Na(+)-H+ exchange, is a common interactor for merlin and ERM (MERM) proteins. *J. Biol. Chem.* **273**, 1273–1276.
- Gary, R. & Bretscher, A. (1995). Ezrin self-association involves binding of an N-terminal domain to a normally masked C-terminal domain that includes the F-actin binding site. *Mol. Biol. Cell*, **6**, 1061–1075.
- Turunen, O., Wahlstrom, T. & Vaehri, A. (1994). Ezrin has a COOH-terminal actin-binding site that is conserved in the ezrin protein family. *J. Cell Biol.* **126**, 1445–1453.
- Pestonjampasp, K., Amieva, M. R., Strassel, C. P., Nauseef, W. M., Furthmayr, H. & Luna, E. J. (1995). Moesin, ezrin, and p205 are actin-binding proteins associated with neutrophil plasma membranes. *Mol. Biol. Cell*, **6**, 247–259.
- Cohen, C. & Parry, D. A. D. (1986). α -Helical coiled coils—a widespread motif in proteins. *Trends Biochem. Sci.* **11**, 245–248.
- Hoeflich, K. P., Tsukita, S., Hicks, L., Kay, C. M. & Ikura, M. (2003). Insights into a single rod-like helix in activated radixin required for membrane-cytoskeletal cross-linking. *Biochemistry*, **42**, 11634–11641.
- Trofatter, J. A., MacCollin, M. M., Rutter, J. L., Murrell, J. R., Duyao, M. P., Parry, D. M. *et al.* (1993). A novel moesin-, ezrin-, radixin-like gene is a candidate for the neurofibromatosis 2 tumor suppressor. *Cell*, **72**, 791–800.
- Rouleau, G. A., Merel, P., Lutchman, M., Sanson, M., Zucman, J., Marineau, C. *et al.* (1993). Alteration in a new gene encoding a putative membrane-organizing protein causes neuro-fibromatosis type 2. *Nature*, **363**, 515–521.
- Finnerty, C. M., Chambers, D., Ingraffea, J., Faber, H. R., Karplus, P. A. & Bretscher, A. (2004). The EBP50-moesin interaction involves a binding site regulated by direct masking on the FERM domain. *J. Cell Sci.* **117**, 1547–1552.
- Terawaki, S., Maesaki, R. & Hakoshima, T. (2006). Structural basis for NHERF recognition by ERM proteins. *Structure*, **14**, 777–789.
- Hamada, K., Shimizu, T., Yonemura, S., Tsukita, S. & Hakoshima, T. (2003). Structural basis of adhesion-molecule recognition by ERM proteins revealed by the crystal structure of the radixin-ICAM-2 complex. *EMBO J.* **22**, 502–514.
- Garcia-Alvarez, B., de Pereda, J. M., Calderwood, D. A., Ulmer, T. S., Critchley, D., Campbell, I. D. *et al.* (2003). Structural determinants of integrin recognition by talin. *Mol. Cell*, **11**, 49–58.
- Ceccarelli, D. F., Song, H. K., Poy, F., Schaller, M. D. & Eck, M. J. (2006). Crystal structure of the FERM domain of focal adhesion kinase. *J. Biol. Chem.* **281**, 252–259.
- Hamada, K., Shimizu, T., Matsui, T., Tsukita, S. & Hakoshima, T. (2000). Structural basis of the membrane-targeting and unmasking mechanisms of the radixin FERM domain. *EMBO J.* **19**, 4449–4462.
- Shimizu, T., Seto, A., Maita, N., Hamada, K., Tsukita, S. & Hakoshima, T. (2002). Structural basis for neurofibromatosis type 2. Crystal structure of the merlin FERM domain. *J. Biol. Chem.* **277**, 10332–10336.
- McClatchey, A. I. & Giovannini, M. (2005). Membrane organization and tumorigenesis—the NF2 tumor suppressor. *Merlin. Genes Dev.* **19**, 2265–2277.
- Miller, K. G. (2003). A role for moesin in polarity. *Trends Cell Biol.* **13**, 165–168.
- Lupas, A., Van Dyke, M. & Stock, J. (1991). Predicting coiled coils from protein sequences. *Science*, **252**, 1162–1164.
- Fievet, B. T., Gautreau, A., Roy, C., Del Maestro, L., Mangeat, P., Louvard, D. & Arpin, M. (2004). Phosphoinositide binding and phosphorylation act sequentially in the activation mechanism of ezrin. *J. Cell Biol.* **164**, 653–659.
- Edwards, S. D. & Keep, N. H. (2001). The 2.7 Å crystal structure of the activated FERM domain of moesin: an analysis of structural changes on activation. *Biochemistry*, **40**, 7061–7068.
- Dransfield, D. T., Bradford, A. J., Smith, J., Martin, M., Roy, C., Mangeat, P. H. & Goldenring, J. R. (1997). Ezrin is a cyclic AMP-dependent protein kinase anchoring protein. *EMBO J.* **16**, 35–43.
- Gronholm, M., Vossebein, L., Carlson, C. R., Kujapanula, J., Teesalu, T., Alftan, K. *et al.* (2003). Merlin links to the cAMP neuronal signaling pathway by

- anchoring the R β subunit of protein kinase A. *J. Biol. Chem.* **278**, 41167–41172.
34. Skehel, J. J. & Wiley, D. C. (2000). Receptor binding and membrane fusion in virus entry: the influenza hemagglutinin. *Annu. Rev. Biochem.* **69**, 531–569.
 35. Krieg, J. & Hunter, T. (1992). Identification of the two major epidermal growth factor-induced tyrosine phosphorylation sites in the microvillar core protein ezrin. *J. Biol. Chem.* **267**, 19258–19265.
 36. Bretscher, A. (1989). Rapid phosphorylation and reorganization of ezrin and spectrin accompany morphological changes induced in A-431 cells by epidermal growth factor. *J. Cell Biol.* **108**, 921–930.
 37. Bretscher, A., Gary, R. & Berryman, M. (1995). Soluble ezrin purified from placenta exists as stable monomers and elongated dimers with masked C-terminal ezrin-radixin-moesin association domains. *Biochemistry*, **34**, 16830–16837.
 38. Nguyen, R., Reczek, D. & Bretscher, A. (2001). Hierarchy of merlin and ezrin N- and C-terminal domain interactions in homo- and heterotypic associations and their relationship to binding of scaffolding proteins EBP50 and E3KARP. *J. Biol. Chem.* **276**, 7621–7629.
 39. Ahronowitz, I., Xin, W., Kiely, R., Sims, K., MacCollin, M. & Nunes, F. P. (2006). Mutational spectrum of the NF2 gene: a meta-analysis of 12 years of research and diagnostic laboratory findings. *Hum. Mutat.*; In the press. (Electronic publication ahead of print).
 40. Fersht, A. (1999). Forces between molecules, and binding energies. In *Structure and Mechanism in Protein Science*, pp. 345–346, W. H. Freeman and Company, New York.
 41. Lodowski, D. T., Barnhill, J. F., Pitcher, J. A., Capel, W. D., Lefkowitz, R. J. & Tesmer, J. J. (2003). Purification, crystallization and preliminary X-ray diffraction studies of a complex between G protein-coupled receptor kinase 2 and G $\beta_1\gamma_2$. *Acta Crystallog. sect. D*, **59**, 936–939.
 42. Lodowski, D. T., Barnhill, J. F., Pyskadlo, R. M., Ghirlando, R., Sterne-Marr, R. & Tesmer, J. J. (2005). The role of G $\beta\gamma$ and domain interfaces in the activation of G protein-coupled receptor kinase 2. *Biochemistry*, **44**, 6958–6970.
 43. Otwinoski, Z. & Minor, W. (1997). Processing of X-ray diffraction data collected in oscillation mode. *Methods Enzymol.* **276**, 307–326.
 44. Vagin, A. & Teplyakov, A. (2000). An approach to multi-copy search in molecular replacement. *Acta Crystallog. sect. D*, **56**, 1622–1624.
 45. Brünger, A. T., Adams, P. D., Clore, G. M., DeLano, W. L., Gros, P., Grosse-Kunstleve, R. W. *et al.* (1998). Crystallography NMR system: A new software suite for macromolecular structure determination. *Acta Crystallog. sect. D*, **54**, 905–921.
 46. Murshudov, G. N., Vagin, A. A. & Dodson, E. J. (1997). Refinement of macromolecular structures by the maximum-likelihood method. *Acta Crystallog. sect. D*, **53**, 240–255.
 47. McCartney, B. M. & Fehon, R. G. (1996). Distinct cellular and subcellular patterns of expression imply distinct functions for the Drosophila homologues of moesin and the neurofibromatosis 2 tumor suppressor, merlin. *J. Cell Biol.* **133**, 843–852.
 48. Hopfner, K. P., Craig, L., Moncalian, G., Zinkel, R. A., Usui, T., Owen, B. A. *et al.* (2002). The Rad50 zinc-hook is a structure joining Mre11 complexes in DNA recombination and repair. *Nature*, **418**, 562–566.
 49. Park, S. Y., Borbat, P. P., Gonzalez-Bonet, G., Bhatnagar, J., Pollard, A. M., Freed, J. H. *et al.* (2006). Reconstruction of the chemotaxis receptor-kinase assembly. *Nature Struct. Mol. Biol.* **13**, 400–407.
 50. Holm, L. & Sander, C. (1995). Dali: a network tool for protein structure comparison. *Trends Biochem. Sci.* **20**, 478–480.
 51. Turunen, O., Sainio, M., Jaaskelainen, J., Carpen, O. & Vaheri, A. (1998). Structure-function relationships in the ezrin family and the effect of tumor-associated point mutations in neurofibromatosis 2 protein. *Biochim. Biophys. Acta*, **1387**, 1–16.

Edited by I. Wilson

(Received 12 September 2006; received in revised form 16 October 2006; accepted 18 October 2006)

Available online 26 October 2006